ACS APPLIED MATERIALS & INTERFACES

Research Article

Cite This: ACS Appl. Mater. Interfaces 2018, 10, 23813−23824

www.acsami.org

Role of Surface Phenolic-OH Groups in N-Rich Porous Organic Polymers for Enhancing the CO_2 Uptake and CO_2/N_2 Selectivity: Experimental and Computational Studies

Sabuj Kanti Das,[†] Piyali Bhanja,[†] Sudipta K. Kundu,[§] Saptarsi Mondal,[‡] and Asim Bhaumik*[,†]

[†]Department of Materials Science and [‡]Department of Spectroscopy, Indian Association for the Cultivation of Science, Jadavpur 700 032, India

[§]Department of Organic Chemistry, Rajabazar Science College, University of Calcutta, 92 A. P. C. Road, Kolkata 700009, India

Supporting Information

ABSTRACT: Design and successful synthesis of phenolic-OH and amine-functionalized porous organic polymers as adsorbent for postcombustion CO_2 uptake from flue gas mixtures along with high CO_2/N_2 selectivity is a very demanding research area in the context of developing a suitable adsorbent to mitigate greenhouse gases. Herein, we report three triazine-based porous organic polymers TrzPOP-1, -2, and -3 through the polycondensation of two triazine rings containing tetraamine and three dialdehydes. These porous organic polymers possess high Brunauer−Emmett−Teller (BET) surface areas of 995, 868, and 772 $m^2\ g^{-1}$, respectively. Out of the three materials, TrzPOP-2 and TrzPOP-3 contain additional phenolic-OH groups along with triazine moiety and secondary amine linkages. At 273 K, TrzPOP-1, -2, and -3 displayed CO_2 uptake capacities of 6.19, 7.51, and 8.54 mmol g^{-1}, respectively, up to 1 bar pressure, which are considerably high among all porous polymers reported till date. Despite the lower BET surface area, TrzPOP-2 and TrzPOP-3 containing phenolic-OH groups showed higher CO_2 uptakes. To understand the CO_2 adsorption mechanism, we have further performed the quantum chemical studies to analyze noncovalent interactions between CO_2 molecules and different polar functionalities present in these porous polymers. TrzPOP-1, -2, and -3 have the capability of selective CO_2 uptake over that of N_2 at 273 K with the selectivity of 61:1, 117:1, and 142:1 by using the initial slope comparing method, along with 108.4, 140.6, and 167.4 by using ideal adsorbed solution theory (IAST) method, respectively. On the other hand, at 298 K, the calculated CO_2/N_2 selectivities in the initial slope comparing method for TrzPOP-1, -2, and -3 are 27:1, 72:1, and 96:1, whereas those using IAST method are 42.1, 75.7, and 94.5, respectively. Cost effective and scalable synthesis of these porous polymeric materials reported herein for selective CO_2 capture has a very promising future for environmental clean-up.

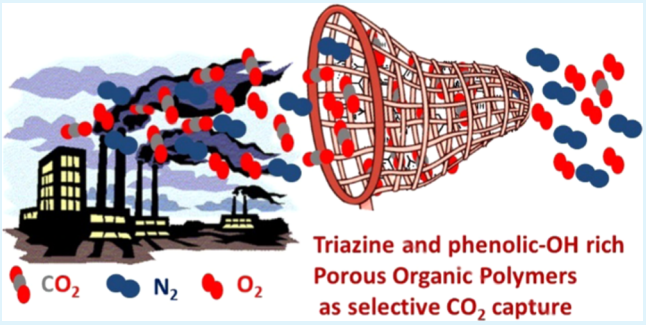

KEYWORDS: *porous organic polymers, N-rich porous surface, phenolic-OH groups, CO_2 uptake, selective CO_2/N_2 adsorption*

1. INTRODUCTION

Global warming is a burning issue today and has deleterious impact on our future existence.[1] Rapid increase of anthropogenic CO_2 emission in the atmosphere resulted in a steady increase of global temperature, which is pushing our green planet toward a big challenge.[2] Sharp increase of our energy demands with the civilization together with the use of fossil fuels like coal and natural gas produces a huge amount of CO_2 (about 80% worldwide), causing steady rise in CO_2 concentration in atmosphere over the years.[3] Flue gas, generated from combustion of fossil fuel, contains roughly 15−16% (by volume) of CO_2.[4] For large postcombustion CO_2 uptake, adsorption capability of the adsorbent material under ambient pressure is very crucial. So CO_2-philic porous material with high Brunauer−Emmett−Teller (BET) surface area is highly demanding for selective postcombustion CO_2 adsorption and storage of CO_2, which can later be utilized in CO_2 fixation plants in processes like reduction of CO_2 into methanol (fuel and solvent).[5] An intensive research effort has been devoted to develop solid adsorbent materials for CO_2 capture and storage.[6] From the inorganic, organic, and organic−inorganic hybrid platforms, materials that showed microporosity together with high specific surface area are desirable for large CO_2 uptake due to micropore filling mechanism.[7] Adsorptive removal of CO_2 by using porous nanomaterials such as porous carbons,[8−10] metal organic frameworks (MOFs),[11,12] covalent organic frameworks,[13−18] hyper-cross-linked polymers,[19,20] hydrogen-bonded organic frameworks,[21] porous organic polymers (POPs),[22−25] and covalent triazene frameworks,[26,27] have attracted wide scale

Received: April 13, 2018
Accepted: June 29, 2018
Published: June 29, 2018

DOI: 10.1021/acsami.8b05849
ACS Appl. Mater. Interfaces 2018, 10, 23813−23824

Scheme 1. Synthetic Pathway for Designing Three Porous Organic Polymers TrzPOP-1, TrzPOP-2, and TrzPOP-3

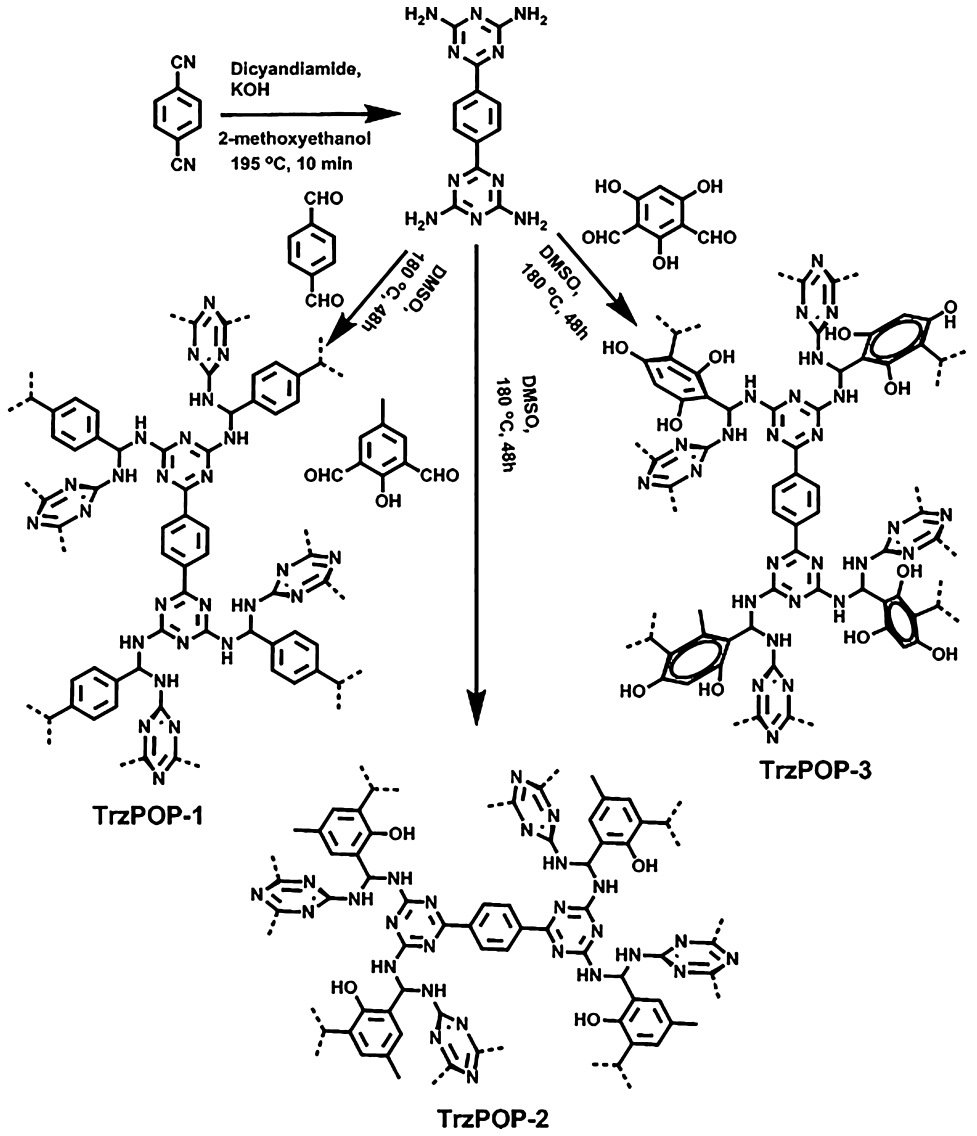

attention in recent times. Remarkable characteristic features of these porous nanomaterials, like high specific surface area, tuneable porosity, introduction of N-rich (basic) sites by using a wide range of monomers, feasibility in postsynthetic functionalization, and robustness in the porous networks, are largely responsible for their high CO_2 uptakes. For high and selective gas adsorption, electronic interaction at the gas−solid interphase is the key factor. CO_2 has higher quadruple moment over N_2, which makes the selective adsorption of CO_2 in the presence of N_2 from flue gas mixture energetically favorable over porous materials bearing polar functional groups at their surfaces.[28,29] In this context, basicity of surface nitrogen atoms incorporated into the porous nanomaterials has been explored for enhancing CO_2 adsorption capacity and CO_2/N_2 selectivity.[30−34]

Acid−base interactions between N-containing basic functional groups of the solid adsorbent and Lewis acidic CO_2 molecule are found to be responsible for higher CO_2 uptakes.[35,36] Qiao et al., in a recent study, made a correlation between CO_2 adsorption capacity and nitrogen contents and found that the total N content cannot account for the greatly increased CO_2 capture by assuming that each N atom can anchor one CO_2 molecule.[32] They claimed that nitrogen introduction could facilitate the hydrogen-bonding interactions between the carbon surface and CO_2 molecules. Thus, N-doping effect in solid adsorbents on CO_2 philicity, as reported in the literature, still needs in-depth evidence or explanation. Besides, the phenolic-OH groups present in the porous network can interact with CO_2 molecule, resulting in higher CO_2 uptake.[37] Fracaroli et al. have reported the interior amine-modified MOF IRMOF-74-III-CH_2NH_2 for selective and high CO_2 uptake.[38] On the basis of computational calculations, Torrisi et al. have reported very high CO_2 uptake over the phenolic-OH functionalized MOF material among the OH−, CO_2H−, NH_2−, and CH_3− functional groups.[39] In this context, Rafigh et al. have recently reported mesoporous chitosan−SiO_2 nanoparticles for large CO_2 adsorption.[40] Chang et al. reported indole-based microporous organic polymers, which can increase the CO_2 uptake via local dipole−π interactions.[41] Vaidhyanathan et al. have also reported a direct observation and quantification of CO_2 binding with an amine-functionalized nanoporous solid material.[40]

DOI: 10.1021/acsami.8b05849
ACS Appl. Mater. Interfaces 2018, 10, 23813−23824

Although the MOFs possess very high surface areas and showed large amount of CO_2 uptakes,[11] their large-scale synthesis and chemical and hydrothermal stability are major drawbacks for bulk scale industrial operation. On the other hand, porous organic polymers (POPs) can be easily synthesized in industrial scale through simple polycondensation reaction between the multifaceted monomers under convenient reaction conditions. POP materials have good hydrothermal stability because of the inherent covalent bonding in the entire polymeric network. Thus, functional group incorporation and postsynthetic modifications are much easier over POPs than MOFs. Considering all above factors along with the existing literature data we can infer that porous organic polymers[37,42,43] bearing heteroatoms like N, O, F, etc. and polar groups like −OH, $-NH_2$, etc. are very useful as solid adsorbents for large CO_2 adsorption together with high CO_2/N_2 selectivity.

Herein, we report −OH and N-rich porous organic polymers synthesized through the polycondensation of two tetraamine-bearing triazine rings as donor moiety and three different dialdehydes (two of them contain phenolic-OH group) as acceptor ligands (Scheme 1). The resultant triazine-based N-rich porous organic polymers TrzPOP-1, -2, and -3 are explored for CO_2 adsorption application. Computational studies have been conducted to understand the interaction between CO_2 molecules and polar heteroatomic porous adsorbent surface. Because of presence of phenolic-OH groups and amine sites in the polymeric network, the significant dipole−quadruple and hydrogen-bonding interactions between polymer surface (polar triazine, amine, and phenolic-OH) and CO_2 molecules are possible. High surface area of the POPs, dipole−quadruple interaction, and hydrogen-bonding interaction made the materials suitable as adsorbent for CO_2 uptake, together with high selectivity for CO_2/N_2. These porous polymeric materials are cost effective, highly scalable, and can be synthesized by simple Schiff base polycondensation reaction without using any expensive or laborious laboratory techniques.

2. EXPERIMENTAL SECTION

2.1. Chemicals. Terephthalonitrile, terephthaldehyde, and dicyandiamide were purchased from Sigma-Aldrich. Phloroglucinol was procured from Spectrochem, India, *p*-cresol from Loba Chemicals, India, and $POCl_3$ from TCI. The organic solvents viz. *N*,*N*-dimethylformamide (anhydrous), dimethylsulfoxide (DMSO), and 2-methoxyethanol were used as received from Spectrochem, India. All reactions were performed without further purification.

2.2. Material Characterizations. The powder X-ray diffraction (XRD) patterns of TrzPOP-1, -2, and -3 were collected in a Bruker AXS D-8 Advanced SWAX diffractometer using Cu Kα (λ = 0.15406 nm) X-ray radiation. Volumetric nitrogen adsorption/desorption isotherms, Brunauer−Emmett−Teller (BET) specific surface area, and porosity analysis of the porous materials were performed using Autosorb 1 (Quantachrome Instruments) at 77 K. Quantitative CO_2 and N_2 adsorption capability of TrzPOP-1, -2, and -3 materials were measured in Micromeritics ASAP 2020 at 273 and 298 K. Virial fittings and Q_{st} plot were obtained using virial method, and this is discussed in Section S1. Single-site Langmuir−Freundlich fittings and necessary equations for selective gas adsorption by using ideal adsorbed solution theory (IAST) method are given in Section S2. Prior to all gas adsorption measurements, samples were washed with plenty of water, followed by solvent extraction in a Soxhlet apparatus for 3 days with MeOH/tetrahydrofuran (THF) (1:1) mixture to remove DMSO and other guest molecules. Finally, the materials have been activated for 24 h at 433 K under vacuum to get guest/solvent-free materials. Nonlocal density functional theory (NLDFT) was employed to obtained pore-size distribution from the N_2 adsorption/desorption isotherms of the TrzPOP-1, -2, and -3 materials. Fourier transform infrared (FTIR) spectra were recorded in a Perkin Elmer Spectrum 100 spectrophotometer to analyze the framework bonding and connectivity in these POPs. The liquid state ^1H and ^{13}C NMR spectra of as-synthesized ligand SL-1 and solid-state ^{13}C magic-angle spinning (MAS) NMR spectrum of three polymers were recorded in a 500 MHz Bruker-Advance II. All solid-state NMR data were taken at a mass frequency of 8 kHz using a 4 nm MAS probe. The morphology and particle size of TrzPOP-1, -2, and -3 were investigated by collecting field emission scanning electron microscopy (FESEM) and high-resolution transmission electron microscopy (HRTEM) images from JEOL JEM 6700 and JEOL 1400 Plus, respectively. TA Instruments SDT Q-600 thermal analyzer has been employed to understand the thermal stability of the porous polymeric networks under nitrogen flow with a temperature ramp of 10 °C min^{-1}. Elemental analysis of the three materials were conducted in a Perkin Elmer 2400 Series II CHN analyzer. All solid-state UV−vis spectra of the POPs were obtained by using the UV-2401PC UV−vis spectrophotometer.

2.3. Synthesis of 1,4-Bis(4,6-diamino-*s*-triazin-2-yl)-benzene (SL-1). Following a literature procedure,[44] we took terephthalonitrile (640 mg, 5 mmol), dicyandiamide (841 mg, 10 mmol), and KOH (100 mg, 1.75 mmol), along with 15 mL of 2-methoxyethanol solvent in a microwave (G-30) vial. The reaction was allowed to proceed at 195 °C under microwave irradiation for 10 min (Scheme 1). Then, the reaction mixture was allowed to cool down to room temperature and poured into hot water. The white precipitate formed was filtered off under hot conditions and washed with plenty of water. The precipitate was washed with methanol and finally with acetone to produce pure compound SL-1 (75% yield). ^1H and ^{13}C NMR data of SL-1 are shown in Figures S1 and S2.

2.4. Synthesis of 2,6-Diformyl-4-methylphenol (Me-OH-DFP). Following a previously reported procedure,[45] Me-OH-DFP was synthesized. In a 100 mL round-bottom flask, 1.08 g of *p*-cresol (0.01 mol) was taken in 5 mL of acetic acid. Then, 2.82 g of hexamethylenetetramine (0.02 mol) and 3 g of paraformaldehyde (0.1 mol) were added to the reaction mixture. The reaction mixture was then allowed to stir for 2 h at 80 °C to get a light-brown viscous mixture. One milliliter of concentrated H_2SO_4 was added dropwise into it after cooling down the mixture to room temperature, followed by refluxing for 30 min. Then, 40 mL of distilled water was added into the resulting solution and a pale-yellow precipitate appeared instantly. The reaction mixture was kept in a refrigerator overnight to enhance the product yield. Then, the product was filtered off and washed with water, followed by a small amount of methanol. Finally, the product was recrystallized from toluene to afford pure Me-OH-DFP (isolated yield 78%). The pure dry Me-OH-DFP has been characterized by ^1H and ^{13}C NMR and FTIR spectroscopic techniques. The ^1H and ^{13}C NMR spectra of Me-OH-DFP are shown in Figures S3 and S4.

2.5. Synthesis of Diformylphloroglucinol (DFP). Following a reported literature,[46] 1 g of anhydrous phloroglucinol (7.9 mmol) was dissolved into 7 mL of dry dioxane taken in a 50 mL round-bottom flask. Then, Vilsmeier reagent[47] was prepared through dropwise addition of 1.6 mL of $POCl_3$ (16.7 mmol) to dry dimethylformamide (1.3 mL, 16.7 mmol) under vigorous stirring for 30 min at room temperature and nitrogen atmosphere. Thereafter, this freshly prepared Vilsmeier reagent was slowly added to the previously prepared phloroglucinol solution under stirring, maintaining room temperature and nitrogen atmosphere. This reaction mixture was continuously stirred for 12 h at room temperature to afford a yellow amorphous solid, and it was cooled to 0 °C. Then, an ice-water slurry was prepared in a 100 mL beaker and the solid mixture was poured into it. The solution was allowed to stir for another 4 h at room temperature and a cream precipitate was formed. This precipitate was collected by filtration and washed with plenty of distilled water. The crude precipitate was then taken in 10 mL of water and refluxed for 5 min. Thereafter, the salmon-colored solid DFP appeared upon cooling to 0 °C and was filtered off. The product was washed with plenty of

DOI: 10.1021/acsami.8b05849
ACS Appl. Mater. Interfaces 2018, 10, 23813−23824

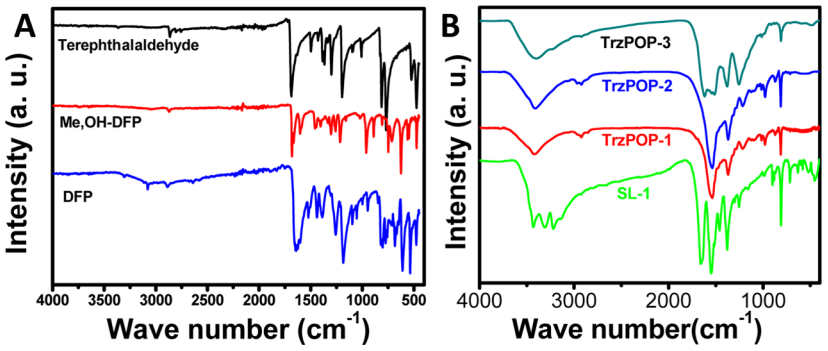

Figure 1. FTIR spectra of three monomer aldehydes (1A) and TrzPOP-1, -2, and -3 along with SL-1 (1B).

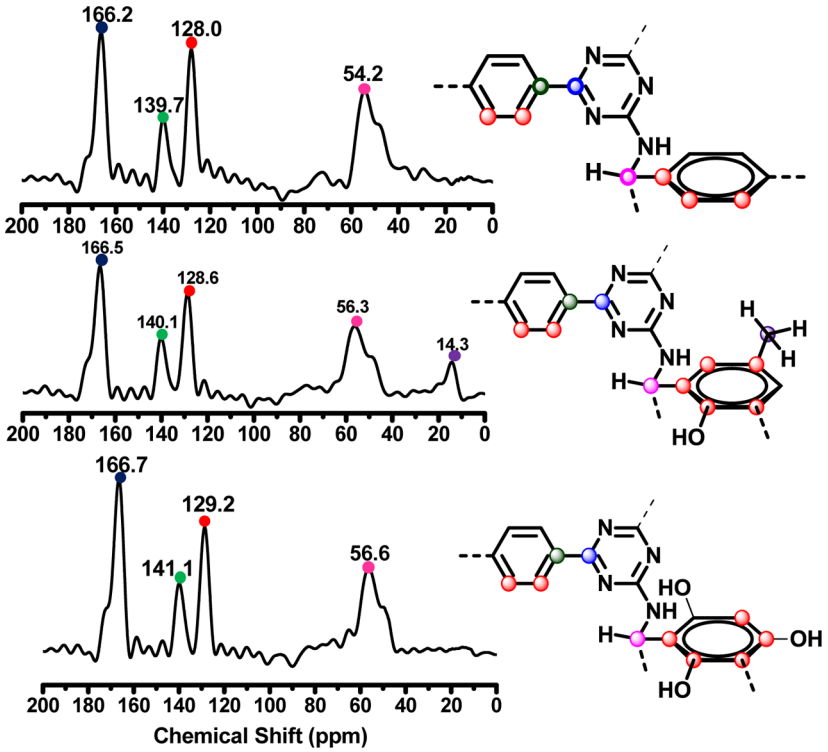

Figure 2. ^{13}C CP/MAS NMR spectra of TrzPOP-1 (upper), TrzPOP-2 (middle), and TrzPOP-3 (lower).

cold water and dried to obtained constant weight (88% isolated yield). The ^{1}H and ^{13}C NMR spectral data of DFP are shown in Figures S5 and S6.

2.6. Synthesis of TrzPOP-1. Triazine-based microporous polymer TrzPOP-1 was synthesized by using the simple poly-condensation reaction[48] between SL-1 and terephthaldehyde. In a typical synthesis, in a 50 mL round-bottom flask, 592.6 mg of SL-1 (2 mmol) and 268.3 mg of terephthaldehyde (2 mmol) were mixed in 20 mL of anhydrous DMSO solvent, followed by stirring with slow increase of temperature under N_2 atmosphere. With the rise of temperature, the starting materials got dissolved and the solution became clear. Then, the reaction mixture was refluxed at 180 °C for 48 h to get solid material. After cooling down to room temperature, the precipitate was then filtered off and washed with plenty of water. To get guest-free TrzPOP-1, material was then further washed with MeOH/THF (1:1) mixture using a Soxhlet apparatus. The material was then washed with acetone and hexane successively to afford very light off-white material (TrzPOP-1), and this was dried under vacuum for 24 h at 433 K.

2.7. Synthesis of TrzPOP-2 and TrzPOP-3. Both TrzPOP-2 (off-white) and TrzPOP-3 (deep-red) materials were synthesized through the above described synthetic procedure (like that of TrzPOP-1). TrzPOP-2 was synthesized through the reaction of SL-1 (592.6 mg, 2 mmol) with Me-OH-DFP (328.3 mg, 2 mmol). TrzPOP-3 has been synthesized through the reaction between SL-1 (592.6 mg, 2 mmol) and DFP (364.2 mg, 2 mmol). A similar washing and activation procedure was followed for these two materials as that for TrzPOP-1 before conducting the adsorption experiments.

2.8. Experimental Procedure of Theoretical Calculations. Three different kinds of 1:1 cluster model system of the porous materials and CO_2 have been optimized using Gaussian 09 suites of the program.[49] For several related systems, weak noncovalent interactions have been investigated using ab initio quantum chemical calculation coupled with atoms in molecules (AIM) analysis.[50,51] It is well known that dispersion-corrected methods are exceptionally good in revealing weak interactions present in this system. Therefore, we have used a range-separated wB97XD dispersion-corrected density functional method (capable of describing both short-range and long-range interactions very reliably) and 3-21G* basis set for the optimization. Frequency calculation has been performed for all structures to ensure that the structures are in local minima. All above calculations have been performed with frozen core approximation, and standard convergence criteria have been imposed during optimization. Stabilization energy (ΔE_{stab}) has been calculated using the following equation

DOI: 10.1021/acsami.8b05849
ACS Appl. Mater. Interfaces 2018, 10, 23813−23824

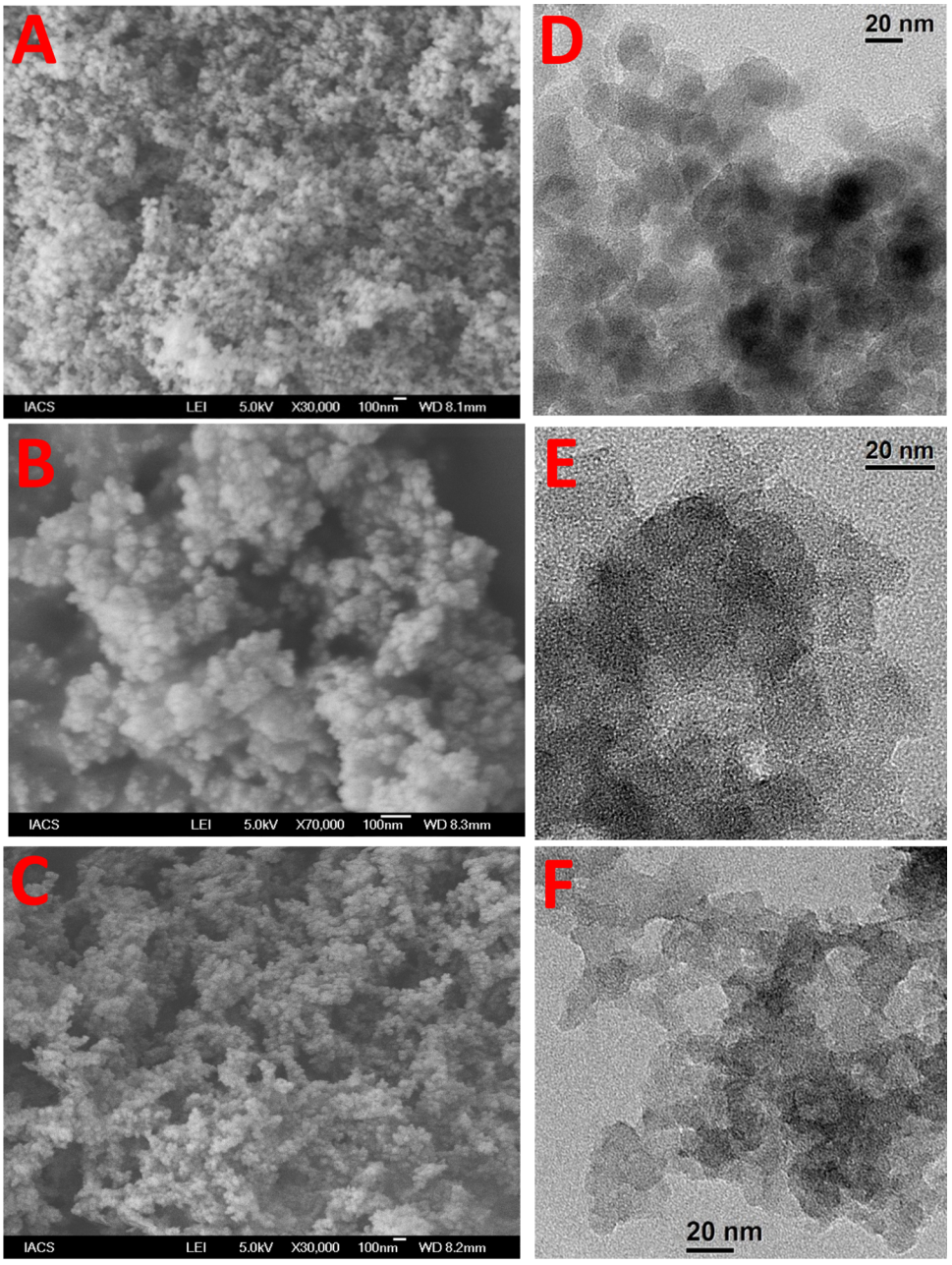

Figure 3. FESEM images of TrzPOP-1 (A), TrzPOP-2 (B), and TrzPOP-3 (C); HRTEM images of TrzPOP-1 (D), TrzPOP-2 (E), and TrzPOP-3 (F).

$$\Delta E_{stab} = E_{clust} - E_{model} - E_{CO_2} \quad (1)$$

where, E_{clust}, E_{model}, and E_{CO_2} are zero-point vibrational energy corrected energies of 1:1 clusters, model system, and CO_2, respectively. To understand the nature of different kinds of noncovalent interactions, we have generated a molecular density map using atoms in molecules (AIM) software and AIM analysis performed afterward.[52−57] Further, we have calculated the electron density (ρ) and Laplacian of electron density ($\nabla^2\rho$, L) at each bond critical point (BCP) to know the nature of the interaction between two interacting atoms. It is important to mention that only those BCPs whose ρ and L are higher than 0.002 and 0.02 au, respectively, have been considered as they confirm the existence of noncovalent interaction. The ellipticity of the interaction (ε) at any particular critical point (CP) has been calculated by the following equation[57]

$$\varepsilon = \frac{\lambda_1}{\lambda_2} - 1 \quad (2)$$

where λ is the negative vector associated with the hessian of ρ at that CP and $\lambda_2 \leq \lambda_1$.

3. RESULTS AND DISCUSSION

3.1. Spectroscopic Analysis. To investigate the completion of the polycondensation reactions and to obtain the structural information on the porous organic polymers, FTIR and ^{13}C cross-polarization (CP)/MAS NMR spectroscopic analyses have been carried out. FTIR spectral analysis of the monomers SL-1, three different aldehydes, and three POP materials are recorded in the range 400−4000 cm^{-1} (Figure 1). The disappearance of the intense sharp aldehydic stretching peak at 1685 cm^{-1} for DFP, 1683 and 1650 cm^{-1} for the

DOI: 10.1021/acsami.8b05849
ACS Appl. Mater. Interfaces 2018, 10, 23813−23824

terephthaldehyde, along with $-NH_2$ deformation band of SL-1 between 1650 and 1660 cm^{-1} confirms the condensation reaction takes place between amine containing ligand and three aldehydes. The presence of a sharp IR band at 1540 cm^{-1} (characteristic band for triazine ring) in both the SL-1 monomer and in all three amine-linked materials indicates the completion of polycondensation reaction.[58] The imine (−C═N−) stretching band at 1620 cm^{-1} is absent, and presence of a very broad band at about 3417 cm^{-1} indicates the formation of three different polymer networks through −C−NH− bonding connection.[59] The solid-state ^{13}C MAS NMR spectrum also confirmed the formation of three polymer materials, represented in Figure 2. Appearance of more down-fielded resonance signals at 166.2, 166.5, and 166.7 ppm suggested the presence of carbon atoms in the triazine rings of TrzPOP-1, -2, and -3, respectively. The sp^2 hybridized aromatic carbon atoms (phenyl ring) present in the polymers are responsible for the resonance signal at 139.7, 140.1, and 141.1 ppm adjacent to the triazine ring of the polymeric materials TrzPOP-1, -2, and -3, respectively. Further, appearance of the NMR signals at 128.0, 128.6, and 129.2 ppm could be assigned to the rest of the sp^2 hybridized carbon atoms present in the phenyl rings of TrzPOP-1, -2, and -3, respectively.[60] The Schiff base condensation reaction can generate two types of C−N linkages like secondary amine (>CH−NH−HC<) or imine (>C═N−C<) linkage. The ^{13}C signal at around 56 ppm could be attributed to the presence of secondary amine linkages, and this is responsible for disordered packing of TrzPOP-1, -2, and -3 nanoparticles.

3.2. Powder XRD, Thermal Stability, and Elemental Analysis. The crystalline nature of the three porous materials have been investigated with the wide-angle powder XRD analysis from 2θ value of 2−50°. The wide-angle powder X-ray diffraction pattern of TrzPOP-1, TrzPOP-2, and TrzPOP-3 materials is shown in Figure S7. The appearance of broad peaks between 2θ value of 15−30° in the PXRD pattern could be attributed to the amorphous nature of the TrzPOPs.[61] These materials are formed through Schiff base condensation polymerization reactions, where secondary amine linkages are formed. The monomers tetraamine and three aldehydes are geometrically unfavorable to construct crystalline covalent organic framework via aminal linkages. Thus, we obtained the amorphous materials with very broad wide-angle peaks. Thermal stability of the porous framework is an essential feature for a good adsorbent material. We have carried out the thermogravimetric analysis (TGA) of TrzPOP-1, -2, and -3 at a heating rate of 10 K per min ramp in the temperature range of 298−1073 K. The TGA profile diagram of these three materials is shown in Figure S8, where the first weight loss at 371 K could be attributed to the evaporation of surface-adsorbed moisture. The weight loss is from 623 to 1073 K for the decomposition of organic polymers network. Thus, thermogravimetric analysis revealed that all three porous materials have good thermal stability. On the other hand, the presence of elements like carbon, hydrogen, and nitrogen is investigated from the CHN analysis. CHN analyses revealed: C = 50.87%, H = 4.93%, and N = 28.99% for TrzPOP-1, C = 53%, H = 4.26%, and N = 26.34% for TrzPOP-2, and C = 48.27%, H = 3.91%, and N = 21.14% for TrzPOP-3. These results revealed that all three POPs are very rich in nitrogen content.

3.3. Microscopic Analysis and UV−vis Spectrum Analysis. The morphological and nanostructural features of these POPs are analyzed through field emission scanning electron microscopy (FESEM) and HRTEM techniques. The FESEM images of TrzPOP-1, TrzPOP-2, and TrzPOP-3 polymers are shown in the Figure 3A−C. The FESEM images show spherical morphology of the three materials. The average particle diameter of TrzPOP-1, TrzPOP-2, and TrzPOP-3 materials are found to be between 17 and 25 nm. The HRTEM images of TrzPOP-1, -2, and 3 are shown in the Figure 3D−F, respectively. HRTEM analysis also confirms the nanosphere-like particle morphology of these three materials, with average particle sizes of 18.87−19.07 nm. The solid-state normalized UV−vis spectra of TrzPOP-1, -2, and -3 are shown in Figure S9. As seen from this figure, TrzPOP-1 displayed peak adsorption maxima at 310 nm, whereas TrzPOP-2 material showed additional two broad peaks at 463 and 642 nm in addition to the peak at 310 nm. The peak at 310 nm could be attributed to the chromophoric triazine containing amine moieties in the POPs. On the other hand, TrzPOP-3 showed the two broad and intense peaks at 398 and 517 nm. Adsorption peaks at the visible region observed for TrzPOP-2 and TrzPOP-3 could be attributed to the presence of phenolic-OH groups, and this spectroscopic result suggested the future potential of these POP materials in light harvesting applications.[62]

3.4. Surface Area and Porosity Measurement. The N_2 adsorption/desorption experiments have been carried out for these three POPs at 77 K to get information on specific surface area, porosity, and pore size distribution (PSD). Respective sorption isotherms are shown in Figure 4A. TrzPOP-1, -2, and -3 displayed type I isotherms according to the classification of IUPAC nomenclature[63] (Figure 4A). The N_2 adsorption/desorption isotherms show very sharp increase of gas adsorption at very low P/P_0, which suggested the microporous nature of the polymer networks. At the high-pressure region, there are sharp increases of all adsorption/desorption isotherms with very small hysteresis loop, which suggested the presence of interparticle porosity in the nanoscale in addition to microporosity. Disordered packing of very small size polymeric nanoparticles (as seen from the FESEM image) could be responsible for this desorption hysteresis.[61] The Brunauer−Emmett−Teller (BET) specific surface areas estimated from these isotherms are 995, 868, and 772 m^2 g^{-1} for TrzPOP-1, -2, and -3, respectively. BET surface areas corresponding to the micropores (S_{micro}) for the three materials were estimated by the using *t*-plot method and these were 372.5, 504.6, and 406.0 m^2 g^{-1}, respectively. Although TrzPOP-2 showed highest S_{micro}, the surface OH density of TrzPOP-3 was higher than that of the former. This could be attributed to higher CO_2 uptake for TrzPOP-3 over that for TrzPOP-2. Applying the nonlocal density functional theory (NLDFT), the pore size distribution (PSD) of the three secondary amine-linked POPs are calculated. The peak pore sizes of these three POPs are 1.7 (TrzPOP-1), 1.5 (TrzPOP-2), and 1.4 nm (TrzPOP-3), which indicates that all three POPs are composed of extra-large sized micropores/super-micropores (Figure 4B). BET surface area, S_{micro}, and PSD data of these materials are listed in Table 1 for clarity.

3.5. CO_2 Storage and CO_2/N_2 Selectivity. For higher CO_2 uptake over the porous adsorbents, along with the high surface area, enhancement of surface CO_2 philicity of the porous materials is extremely important. Porous materials can be functionalized through the incorporation of some heteroatoms as well as different functionalities that are able

DOI: 10.1021/acsami.8b05849
ACS Appl. Mater. Interfaces 2018, 10, 23813−23824

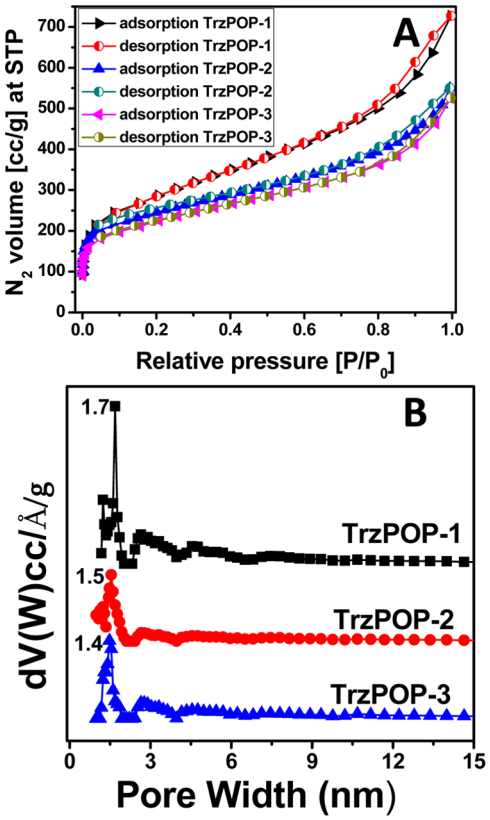

Figure 4. (A) N_2 adsorption/desorption isotherms of TrzPOP-1, TrzPOP-2, and TrzPOP-3. Adsorption points are marked by filled circles and desorption points are marked by empty circles. (B) Pore size distribution plots of TrzPOP-1 (black), TrzPOP-2 (red), and TrzPOP-3 (blue).

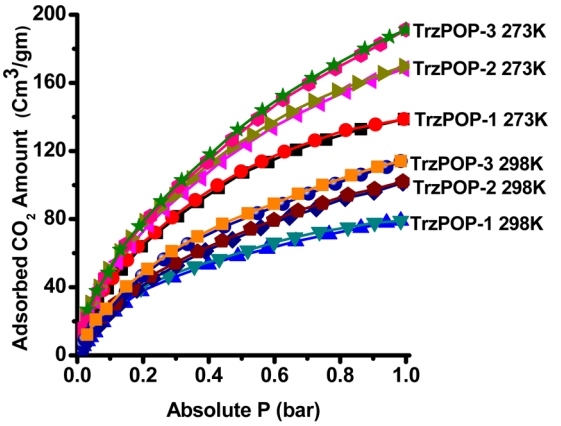

Figure 5. CO_2 uptake of TrzPOP-1, TrzPOP-2, and TrzPOP-3 at 273 and 298 K.

to generate a electrostatic field on the porous surface and into the pore of the polymer network so that CO_2 can interact significantly with the host material through quadruple interaction.[64] Presence of atoms or functional groups in the materials facilitates the dipole−quadruple interaction, which increases the CO_2 affinity toward porous surface. Here, we have explored the secondary amine-linked, large number of triazine rings and phenolic-OH functionalities in the porous polymer network of TrzPOPs for selective and high CO_2 uptake. The CO_2 adsorption isotherms of TrzPOP-1, -2, and -3 at 273 and 298 K are shown in Figure 5. The three POP materials showed very high reversible CO_2 uptakes of up to 1 bar pressure. TrzPOP-1 has the capability of CO_2 uptake of 6.19 and 3.53 mmol g^{-1} at 273 and 298 K under 1 bar pressure, respectively. TrzPOP-2 showed 7.51 mmol g^{-1} CO_2 uptake at up to 1 bar pressure at 273 K and 4.52 mmol g^{-1} at 298 K temperature. On the other hand, TrzPOP-3 showed CO_2 uptakes of 8.54 and 5.09 mmol g^{-1} at 273 and 298 K under 1 bar pressure, respectively. All three materials contain very high density of N atom as the materials are formed through amine linkage and a large number of triazine rings are present in the polymer network. TrzPOP-2 material contains extra −Me and −OH groups, which come from the aldehyde monomer unit. TrzPOP-3 material was designed in such a way that it contains more phenolic −OH groups with respect to those in TrzPOP-2. Although TrzPOP-3 has the lowest surface area, it displayed the highest CO_2 uptake capacity. TrzPOP-1 contains only triazine moiety and secondary amine linkages, and these are also present in TrzPOP-2 and -3. Despite its highest surface area, TrzPOP-1 showed the lowest CO_2 uptake capacity among these three materials, suggesting the key role of phenolic-OH functionalities for large CO_2 uptake.

The sharp increase of CO_2 adsorption isotherm at the low-pressure region is the indication of the presence of strong polarizing sites in the porous organic polymeric solid adsorbents.[65] To investigate this phenomenon, we have calculated the isoelectric heat of adsorption (Q_{st}) values of the three materials using virial Method. The Q_{st} plot of the three materials is shown in Figure S10a. The obtained Q_{st} values are 29, 34, and 37 kJ mol^{-1} for TrzPOP-1, TrzPOP-2, and TrzPOP-3, respectively. The CO_2 felicity with the porous surface of TrzPOP-3 is higher than that of the other two materials, which indicated the possibility of more selective CO_2 uptake over that of N_2.[23] The CO_2 adsorption isotherms (symbol) of TrzPOP-1, -2, and -3 at 273 and 298 K with the virial equation fits (lines) are shown in Figure S10b−d, respectively.

The Q_{st} values and computational study indicate a significant interaction present between CO_2 molecules and surface of the materials. These results lead us to investigate the selectivity of CO_2 over that of N_2, which can provide useful information for the efficiency of the adsorbent material in gas separation

Table 1. Surface Area, Pore Size Distribution (PSD), CO_2 Uptake, Binding Affinity, and Selectivity (CO_2/N_2) for Three POP Materials

				CO_2 adsorption (mmol g^{-1})		CO_2/N_2 selectivity		CO_2/N_2 selectivity-(IAST method)		Q_{st} (kJ mol^{-1})
porous organic polymers	BET (m^2 g^{-1})	S_{micro} (m^2 g^{-1})	PSD (nm)	273 K	298 K	273 K	298 K	273 K	298 K	CO_2
TrzPOP-1	995	372.5	1.7	6.19	3.53	61:1	27:1	108.4	42.1	29
TrzPOP-2	868	504.6	1.5	7.51	4.52	117:1	72:1	140.6	75.7	34
TrzPOP-3	772	406.0	1.4	8.54	5.09	142:1	96:1	167.4	94.5	37

DOI: 10.1021/acsami.8b05849
ACS Appl. Mater. Interfaces 2018, 10, 23813−23824

application. The preferential CO_2 uptakes over those of N_2 for TrzPOP-1, -2, and -3 are quite evident from the volumetric physisorption isotherms with pure gas at 273 as well as 298 K (Figures 6, 7, and 8, respectively). TrzPOP-1, -2, and -3 have

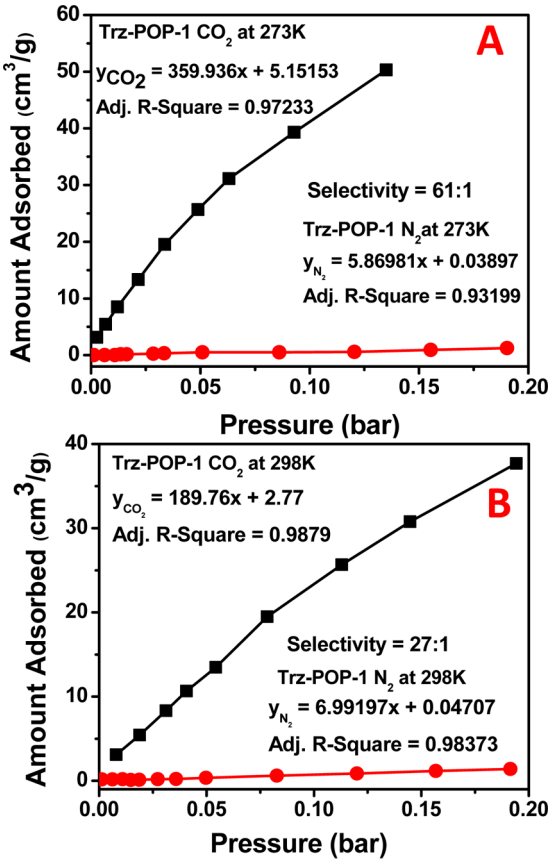

Figure 6. CO_2/N_2 selectivity of TrzPOP-1 at 273 K (A) and at 298 K (B).

the capability of selective CO_2 uptake over that of N_2 at 273 K with the selectivity of 61:1, 117:1, and 142:1, respectively. Further, the calculated CO_2/N_2 selectivities for TrzPOP-1, TrzPOP-2, and TrzPOP-3 are 27:1, 72:1, and 96:1, respectively, at 298 K. Selectivity of CO_2 uptake over that of N_2 was also calculated using IAST model[66] (Figures 9, 10, and 11), where at 273 K, the selectivity values of TrzPOP-1, -2, and -3 were 108.4, 140.6, and 167.4, respectively, whereas at 298 K, TrzPOP-1, -2, and -3 showed the selectivity values of 42.1, 75.7, and 94.5, respectively. The selective uptakes of CO_2 over those of N_2 by TrzPOP 1, -2, and -3 were estimated toward the separation of binary gas mixture using IAST method in which the single-component CO_2 and N_2 adsorption isotherms at 273 and 298 K were fitted to obtain the fitting parameters on the basis of the single-site Langmuir−Freundlich equation (Figures S11−S16). Surface area (of the total and of micropore) of the materials, CO_2 uptake, CO_2/N_2 selectivity, and Q_{st} values are also listed in Table 1.

The CO_2 uptake of these three polymers, mainly TrzPOP-3, is very high and comparable to the highest CO_2 storage capacity of different classes of porous nanomaterials composed of organic, inorganic, and organic−inorganic hybrid frameworks. Comparative adsorption data of these materials are listed in Table S1.

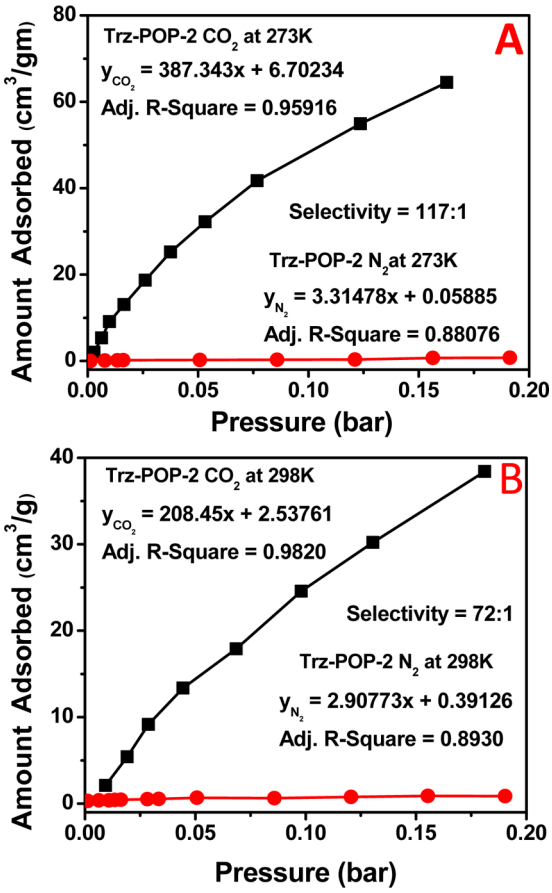

Figure 7. CO_2/N_2 selectivity of TrzPOP-2 at 273 K (A) and at 298 K (B).

3.6. Recycling Efficiency of TrzPOPs in CO_2 Capture. Our experimental data suggested that TrzPOP-3 has the highest CO_2 uptake capacity as well as the highest CO_2/N_2 adsorption selectivity. For practical application in compatibility check and reusability, TrzPOP-3 was employed as the representative adsorbent for four consecutive CO_2 uptake cycles at 273 and 298 K up to 1 bar pressure (Figures 12, S17 and S18). As seen from Figure 12, no significant changes in CO_2 uptake values were observed after four consecutive adsorption cycles. To perform the recycling experiment, the TrzPOP-3 sample was degassed at 433 K for 5 h under high vacuum before the quantitative CO_2 uptake measurement for each cycle. Very high retention of CO_2 uptakes for four repetitive adsorption cycles suggested high reusability of these TrzPOPs in CO_2 storage application.

3.7. Quantum Chemical Analysis. To perform the quantum chemical analysis, we have selected a repeating unit of TrzPOP-2 as the model system in which secondary amine linkage, triazine moiety, as well as phenolic-OH functionality is present. To understand the reason behind the high CO_2 uptake by the newly synthesized POPs, we have optimized the 1:1 cluster of the model system and CO_2 and created a molecular density map (Figure 13a−c). The energetics ρ and L for different weak noncovalent interactions have been listed in the Table 2. It can be clearly seen that the cluster 1 (Figure 13a) is more stable (ΔE_{stab} = 10.96 kcal mol^{-1}) compared with cluster 2 (ΔE_{stab} = 7.00 kcal mol^{-1}, Figure 13b) and cluster 3 (ΔE_{stab} = 6.06 kcal mol^{-1}, Figure 13c). The presence of the (3, −1) critical points, i.e., BCPs with positive and higher ρ and L

DOI: 10.1021/acsami.8b05849
ACS Appl. Mater. Interfaces 2018, 10, 23813−23824

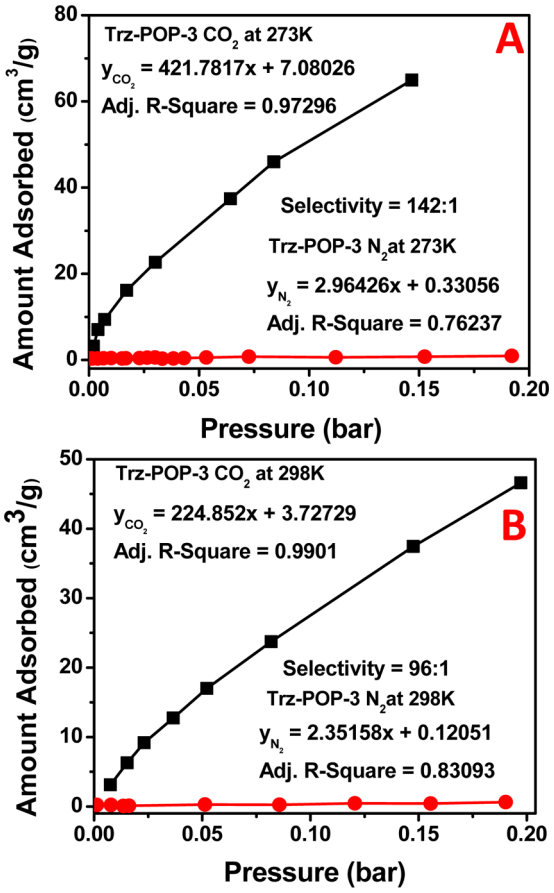

Figure 8. CO_2/N_2 selectivity of TrzPOP-3 at 273 K (A) and at 298 K (B).

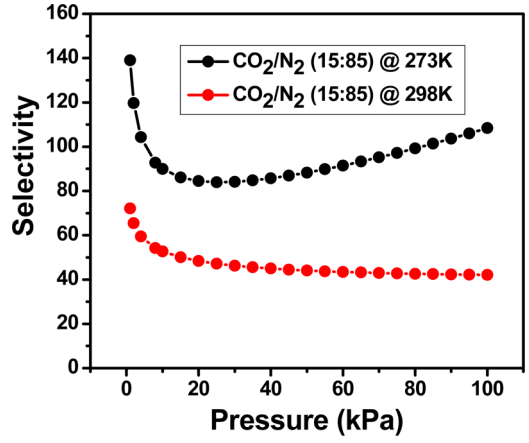

Figure 9. CO_2/N_2 selectivity (IAST method) of TrzPOP-1 at 273 K (black) and at 298 K (red).

values compared with 0.002 and 0.02 au confirmed the existence of two N−H···O and one N···C interaction in the cluster 1 (Figure 13a), N−H···O, C−H···O, O···C, and N···C interaction in cluster 2 (Figure 13b), and O−H···O and C−H···O interactions in cluster 3 (Figure 13c) between the model system and CO_2. These types of noncovalent interactions have already been reported in the literature for weakly bonded complexes.[67]

The values of ρ and L for all BCPs reveal that both the N−H···O and O−H···O interactions[31] are very strong with very high (compared to other weak interactions) ρ and L values

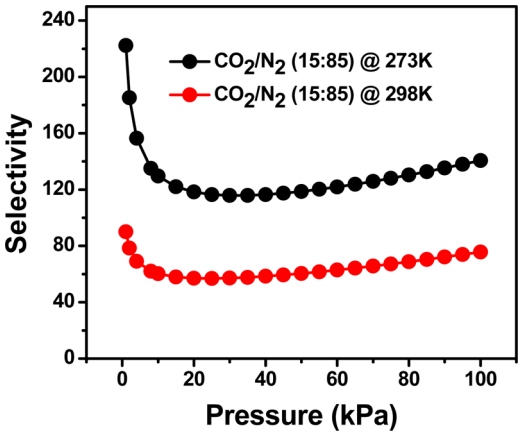

Figure 10. CO_2/N_2 selectivity (IAST method) of TrzPOP-2 at 273 K (black) and at 298 K (red).

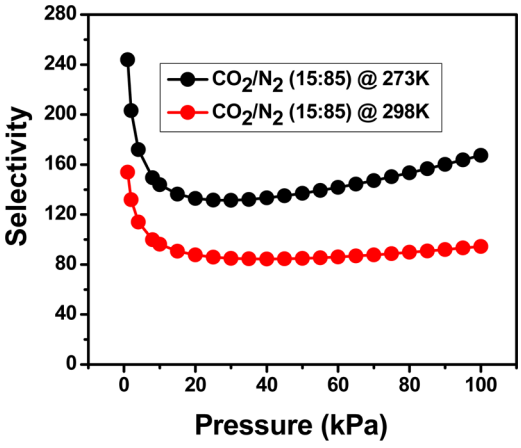

Figure 11. CO_2/N_2 selectivity (IAST method) of TrzPOP-3 at 273 K (black) and at 298 K (red).

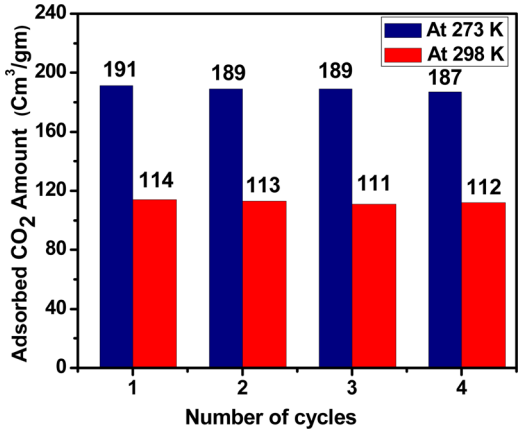

Figure 12. Recycling efficiency of TrzPOP-3 for the CO_2 adsorption at 273 and 298 K.

(Table 2). Other interactions N···C, O···C, and C−H···O are relatively weaker, but there is a fair probability that they also exist in the material as their ρ and L values are higher compared with the limit to be considered as weak interaction. On the other hand, we have tabulated the values of ε also for all interactions (Table 2), which merely reflects the anisotropy of the curvature of the electron density at a particular CP. More the values of ε, more is the accumulation of the electron

DOI: 10.1021/acsami.8b05849
ACS Appl. Mater. Interfaces 2018, 10, 23813−23824

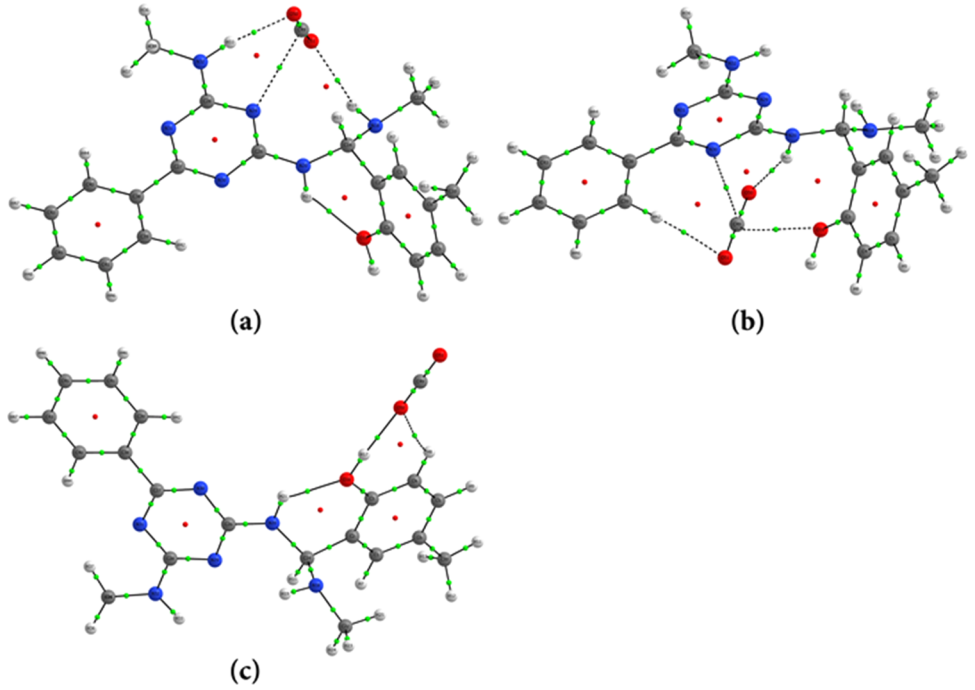

Figure 13. Electron density map of cluster 1 (a), cluster 2 (b), and cluster 3 (c) optimized at wB97XD/3-21G* level theory where C, H, N, and O atoms are represented in gray, white, blue, and red spheres, respectively. The BCPs and ring critical points are represented in small green and red spheres, respectively. The weak noncovalent interaction between the model system and CO_2 has been shown as a black dotted line.

Table 2. List of Stabilization Energy Values (ΔE_{stab}, kcal mol^{-1}) of the Clusters, Electron Density (ρ, au), Laplacian (L, au) and Ellipticity of the Weak Interaction en the 1:1 Cluster of the Model System and CO_2 for all Optimized Geometries Calculated at Wb97XD321G* Level of Theory

interaction (model CO_2)	ΔE_{stab}	ρ	L	ε
	Cluster 1			
N−H···O	10.96	0.0194	0.0922	0.064
N−H···O		0.0145	0.0799	0.267
N···C		0.0182	0.0631	0.405
	Cluster 2			
N−H···O	7.00	0.0239	0.0992	0.028
C−H···O		0.0113	0.0563	0.111
O···C		0.0118	0.0580	1.437
N···C		0.0095	0.0350	0.670
	Cluster 3			
O−H···O	6.06	0.0280	0.1113	0.010
C−H···O		0.0063	0.0340	0.274

density at a perpendicular direction of the interacting plane at that CP and more is the π character. Hence, it can be clearly observed that the values of ε are higher for the weak interactions like N···C, O···C, and C−H···O. They possess a high π bond character, whereas strong interactions like N−H···O and O−H···O have a relatively low ε value, which reflected their cylindrical symmetry and hence, single bond character.

4. CONCLUSIONS

Three triazine-based porous polymers TrzPOP-1, -2, and -3 were successfully synthesized by one-step Schiff base polycondensation reactions. Out of these three, the latter two materials contained additional phenolic-OH groups in addition to triazine moieties in the porous polymer frameworks. These materials are highly porous and having very high BET surface areas of 995, 868, and 772 m^2 g^{-1}, respectively. TrzPOP-3 showed a remarkable CO_2 uptake of 8.54 and 5.09 mmol g^{-1} at 273 and 298 K under 1 bar pressure, respectively. TrzPOP-1, -2, and -3 have the capability for selective CO_2 uptake over N_2 at 273 and 298 K with the selectivities of 61:1, 117:1, and 142:1 and 27:1, 72:1, and 96:1 respectively. Using the IAST method, the calculated CO_2/N_2 selectivity of TrzPOP-1, -2, and -3 at 273 and 298 K are 108.4, 140.6, and 167.4 and 42.1, 75.7, and 94.5, respectively. We have investigated the possibility of different kinds of weak noncovalent interactions pf 1:1 clusters of the model system for the adsorbent and CO_2 to understand the higher CO_2 uptake with the increasing electrophilic functional groups. Ab initio quantum chemical calculations coupled with AIM analysis confirmed the existence of strong N−H···O and O−H···O hydrogen-bonding interactions as well as weak N···C, O···C, and C−H···O interactions. Hence, higher CO_2 uptakes could be attributed to several weak noncovalent interactions between CO_2 and the model system studied. High-surface-area porous organic polymers with phenolic-OH and N-rich surfaces played a key role in large CO_2 uptake, and thus these triazine and phenolic-OH rich POPs have a huge potential to be explored as adsorbent in postcombustion carbon dioxide capture on the industrial scale to make our environment clean and sustainable.

■ ASSOCIATED CONTENT

Supporting Information

The Supporting Information is available free of charge on the ACS Publications website at DOI: 10.1021/acsami.8b05849.

^{1}H and ^{13}C NMR spectra of monomers, wide angle XRD, UV−visible spectra and TG/DTA profiles of TrzPOP-1, -2, and -3 materials, and calculations for the isosteric heat of adsorptions over these adsorbents (PDF)

DOI: 10.1021/acsami.8b05849
ACS Appl. Mater. Interfaces 2018, 10, 23813−23824

AUTHOR INFORMATION

Corresponding Author

*E-mail: msab@iacs.res.in.

ORCID

Sabuj Kanti Das: 0000-0003-1284-385X

Asim Bhaumik: 0000-0002-4907-7418

Author Contributions

The manuscript was written through contributions of all authors. All authors have given approval to the final version of the manuscript.

Notes

The authors declare no competing financial interest.

ACKNOWLEDGMENTS

S.K.D. wishes to acknowledge UGC New Delhi for Senior Research Fellowship. P.B. wishes to acknowledge CSIR, New Delhi for a Senior Research Fellowship.

REFERENCES

(1) Davis, S. J.; Caldeira, K.; Matthews, H. D. Future CO_2 emissions and climate change from existing energy infrastructure. *Science* **2010**, *329*, 1330−1333.

(2) Powell, C. E.; Qiao, G. G. Polymeric CO_2/N_2 gas separation membranes for the capture of carbon dioxide from power plant flue gases. *J. Membr. Sci.* **2006**, *279*, 1−49.

(3) Quadrelli, R.; Peterson, S. The energy-climate challenge: Recent trends in CO_2 emissions from fuel combustion. *Energy Policy* **2007**, *35*, 5938−5952.

(4) Granite, E. J.; Pennline, H. W. Photochemical Removal of Mercury from Flue Gas. *Ind. Eng. Chem. Res.* **2002**, *41*, 5470−5476.

(5) Kondratenko, E. V.; Mul, G.; Baltrusaitis, J.; Larrazabal, G. O.; Perez-Ramirez, J. Status and perspectives of CO_2 conversion into fuels and chemicals by catalytic, photocatalytic and electrocatalytic processes. *Energy Environ. Sci.* **2013**, *6*, 3112−3135.

(6) Niu, M.; Yang, H. M.; Zhang, X. C.; Wang, Y. T.; Tang, A. D. Amine-Impregnated Mesoporous Silica Nanotube as an Emerging Nanocomposite for CO_2 Capture. *ACS Appl. Mater. Interfaces* **2016**, *8*, 17312−17320.

(7) Cong, H. L.; Zhang, M. R.; Chen, Y. L.; Chen, K.; Hao, Y. J.; Zhao, Y. F.; Feng, L. Highly selective CO_2 capture by nitrogen enriched porous carbons. *Carbon* **2015**, *92*, 297−304.

(8) Liu, X.; Li, H.; Zhang, Y.; Xu, B.; A, S.; Xia, H.; Mu, Y. Enhanced carbon dioxide uptake by metalloporphyrin based microporous covalent triazine framework. *Polym. Chem.* **2013**, *4*, 2445−2448.

(9) Bikshapathi, M.; Sharma, A.; Sharma, A.; Verma, N. Preparation of Carbon Molecular Sieves from Carbon Micro and Nanofibers for Sequestration of CO_2. *Chem. Eng. Res. Des.* **2011**, *89*, 1737−1746.

(10) Guangzhi, Y.; Jinyu, Y.; Yuhua, Y.; Zhihong, T.; Guang, Y. D.; Junhe, Y. Preparation and CO_2 Adsorption Properties of Porous Carbon from Camphor Leaves by Hydrothermal Carbonization and Sequential Potassium Hydroxide Activation. *RSC Adv.* **2017**, *7*, 4152−4160.

(11) Trickett, C. A.; Helal, A.; Al-Maythalony, B. A.; Yamani, Z. H.; Cordova, K. E.; Yaghi, O. M. The Chemistry of Metal-Organic Frameworks for CO_2 Capture, Regeneration and Conversion. *Nat. Rev. Mater.* **2017**, *2*, No. 17045.

(12) Das, S. K.; Chatterjee, S.; Bhunia, S.; Mondal, A.; Mitra, P.; Kumari, V.; Pradhan, A.; Bhaumik, A. A New Strongly Paramagnetic Cerium-Containing Microporous MOF for CO_2 Fixation Under Ambient Conditions. *Dalton Trans.* **2017**, *46*, 13783−13792.

(13) Zeng, Y.; Zou, R.; Zhao, Y. Covalent Organic Frameworks for CO_2 Capture. *Adv. Mater.* **2016**, *28*, 2855−2873.

(14) Gomes, R.; Bhanja, P.; Bhaumik, A. A Triazine-Based Covalent Organic Polymer for Efficient CO_2 Adsorption. *Chem. Commun.* **2015**, *51*, 10050−10053.

(15) Huang, N.; Chen, X.; Krishna, R.; Jiang, D. Two-Dimensional Covalent Organic Frameworks for Carbon Dioxide Capture through Channel-Wall Functionalization. *Angew. Chem., Int. Ed.* **2015**, *54*, 2986−2990.

(16) Li, Z.; Feng, X.; Zou, Y.; Zhang, Y.; Xia, H.; Liu, X.; Mu, Y. A 2D Azine-Linked Covalent Organic Framework for Gas Storage Applications. *Chem. Commun.* **2014**, *50*, 13825−13828.

(17) Zou, C.; Li, Q. Q.; Hua, Y. Y.; Zhou, B. H.; Duan, J. G.; Jin, W. Q. Mechanical Synthesis of COF Nanosheet Cluster and Its Mixed Matrix Membrane for Efficient CO_2 Removal. *ACS Appl. Mater. Interfaces* **2017**, *9*, 29093−29100.

(18) Errahali, M.; Gatti, G.; Tei, L.; Paul, G.; Rolla, G. A.; Canti, L.; Fraccarollo, A.; Cossi, M.; Comotti, A.; Sozzani, P.; Marchese, L. Microporous Hyper-Cross-Linked Aromatic Polymers Designed for Methane and Carbon Dioxide Adsorption. *J. Phys. Chem. C* **2014**, *118*, 28699−28710.

(19) Dawson, R.; Cooper, A. I.; Adams, D. J. Chemical Functionalization Strategies for Carbon Dioxide Capture in Microporous Organic Polymers. *Polym. Int.* **2013**, *62*, 345−352.

(20) Wang, H.; Li, B.; Wu, H.; Hu, T.-L.; Yao, Z.; Zhou, W.; Xiang, S.; Chen, B. A Flexible Microporous Hydrogen-Bonded Organic Framework for Gas Sorption and Separation. *J. Am. Chem. Soc.* **2015**, *137*, 9963−9970.

(21) Bandyopadhyay, S.; Anil, A. G.; James, A.; Patra, A. Multifunctional Porous Organic Polymers: Tuning of Porosity, CO_2, and H_2 Storage and Visible-Light-Driven Photocatalysis. *ACS Appl. Mater. Interfaces* **2016**, *8*, 27669−27678.

(22) Zou, L.; Sun, Y.; Che, S.; Yang, X.; Wang, X.; Bosch, M.; Wang, Q.; Li, H.; Smith, M.; Yuan, S.; Perry, Z.; Zhou, H. C. Porous Organic Polymers for Post-Combustion Carbon Capture. *Adv. Mater.* **2017**, *29*, No. 1700229.

(23) Mondal, S.; Kundu, S. K.; Bhaumik, A. A Facile Approach for The Synthesis Of Hydroxyl-Rich Microporous Organic Networks for Efficient CO_2 Capture and H_2 Storage. *Chem. Commun.* **2017**, *53*, 2752−2755.

(24) Sekizkardes, A. K.; Culp, J. T.; Islamoglu, T.; Marti, A.; Hopkinson, D.; Myers, C.; El-Kaderi, H. M.; Nulwala, H. B. An Ultra-Microporous Organic Polymer for High Performance Carbon Dioxide Capture and Separation. *Chem. Commun.* **2015**, *51*, 13393−13396.

(25) Zhu, Y. L.; Zhang, W. Reversible Tuning of Pore Size And CO_2 Adsorption in Azobenzene Functionalized Porous Organic Polymers. *Chem. Sci.* **2014**, *5*, 4957−4961.

(26) Wang, K.; Huang, H.; Liu, D.; Wang, C.; Li, J.; Zhong, C. Covalent Triazine-Based Frameworks with Ultramicropores and High Nitrogen Contents for Highly Selective CO_2 Capture. *Environ. Sci. Technol.* **2016**, *50*, 4869−4876.

(27) Park, K.; Lee, K.; Kim, H.; Ganesan, V.; Cho, K.; Jeong, S. K.; Yoon, S. Preparation of Covalent Triazine Framework with the Imidazolium Cation Embedded in Basic Sites and Its application for CO_2 Capture. *J. Mater. Chem. A* **2017**, *5*, 8576−8582.

(28) Shen, C.; Yu, H.; Wang, Z. Synthesis Of 1,3,5,7-Tetrakis(4-Cyanatophenyl) Adamantane and its Microporous Polycyanurate Network for Adsorption Of Organic Vapors, Hydrogen and Carbon Dioxide. *Chem. Commun.* **2014**, *50*, 11238−11241.

(29) Khajehpour, M.; Kauffman, J. F. Emission Peak Shifts of a Dipolar Solute Dissolved in Nondipolar Solvents: A Quantitative Measure of Quadrupole-Dipole Interactions in Supercritical CO_2. *J. Phys. Chem. A* **2000**, *104*, 9512−9517.

(30) Lee, Y. J.; Talapaneni, S. N.; Coskun, A. Chemically Activated Covalent Triazine Frameworks with Enhanced Textural Properties for High Capacity Gas Storage. *ACS Appl. Mater. Interfaces* **2017**, *9*, 30679−30685.

(31) Rabbani, M. G.; El-Kaderi, H. M. Synthesis and Characterization of Porous Benzimidazole-Linked Polymers and Their Performance in Small Gas Storage and Selective Uptake. *Chem. Mater.* **2012**, *24*, 1511−1517.

(32) Xing, W.; Liu, C.; Zhou, Z.; Zhang, L.; Zhou, J.; Zhuo, S.; Yan, Z.; Gao, H.; Wang, G.; Qiao, S. Z. Superior CO_2 uptake of N-doped

DOI: 10.1021/acsami.8b05849
ACS Appl. Mater. Interfaces 2018, 10, 23813−23824

activated carbon through hydrogen-bonding interaction. *Energy Environ. Sci.* **2012**, *5*, 7323−7327.
(33) Wang, J.; Senkovska, I.; Oschatz, M.; Lohe, M. R.; Borchardt, L.; Heerwig, A.; Liu, Q.; Kaskel, S. Imine-Linked Polymer-Derived Nitrogen-Doped Microporous Carbons with Excellent CO_2 Capture Properties. *ACS Appl. Mater. Interfaces* **2013**, *5*, 3160−3167.
(34) Sevilla, M.; Valle-Vigon, P.; Fuertes, A. B. N-Doped Polypyrrole-Based Porous Carbons for CO_2 Capture. *Adv. Funct. Mater.* **2011**, *21*, 2781−2787.
(35) Adeniran, B.; Mokaya, R. Is N-Doping in Porous Carbons Beneficial for CO_2 Storage? Experimental Demonstration of the Relative Effects of Pore Size and N-Doping. *Chem. Mater.* **2016**, *28*, 994−1001.
(36) Lin, Y.; Kong, C.; Chen, L. Amine-Functionalized Metal-Organic Frameworks: Structure, Synthesis and Applications. *RSC Adv.* **2016**, *6*, 32598−32614.
(37) Katsoulidis, A. P.; Kanatzidis, M. G. Phloroglucinol Based Microporous Polymeric Organic Frameworks with -OH Functional Groups and High CO_2 Capture Capacity. *Chem. Mater.* **2011**, *23*, 1818−1824.
(38) Fracaroli, A. M.; Furukawa, H.; Suzuki, M.; Dodd, M.; Okajima, S.; Gandara, F.; Reimer, J. A.; Yaghi, O. M. Metal-Organic Frameworks with Precisely Designed Interior for Carbon Dioxide Capture in the Presence of Water. *J. Am. Chem. Soc.* **2014**, *136*, 8863−8866.
(39) Torrisi, A.; Bell, R. G.; Mellot-Draznieks, C. Functionalized MOFs for Enhanced CO_2 Capture. *Cryst. Growth Des.* **2010**, *10*, 2839−2841.
(40) Rafigh, S. M.; Heydarinasab, A. Mesoporous Chitosan-SiO_2 Nanoparticles: Synthesis, Characterization, and CO_2 Adsorption Capacity. *ACS Sustainable Chem. Eng.* **2017**, *5*, 10379−10386.
(41) Chang, G.; Shang, Z.; Yu, T.; Yang, L. Rational Design of a Novel Indole-Based Microporous Organic Polymer: Enhanced Carbon Dioxide Uptake Via Local Dipole- π Interactions. *J. Mater. Chem. A* **2016**, *4*, 2517−2523.
(42) Vaidhyanathan, R.; Iremonger, S. S.; Shimizu, G. K. H.; Boyd, P. G.; Alavi, S.; Woo, T. K. Direct Observation and Quantification of CO_2 Binding Within an Amine-Functionalized Nanoporous Solid. *Science* **2010**, *330*, 650−653.
(43) Lu, W.; Yuan, D.; Sculley, J.; Zhao, D.; Krishna, R.; Zhou, H.-C. Sulfonate-Grafted Porous Polymer Networks for Preferential CO_2 Adsorption at Low Pressure. *J. Am. Chem. Soc.* **2011**, *133*, 18126−18129.
(44) Ruiz-Osés, M.; Gonzalez-Lakunza, N.; Silanes, I.; Gourdon, A.; Arnau, A.; Ortega, J. E. Self-Assembly of Heterogeneous Supramolecular Structures with Uniaxial Anisotropy. *J. Phys. Chem. B* **2006**, *110*, 25573−25577.
(45) Qu, J. F.; Chen, D. Y.; LiN, J.; Xu, Q. F.; Li, H.; He, J. H.; Lu, J. M. Coral-inspired nanoscale design of porous SnS_2 for photocatalytic reduction and removal of aqueous Cr (VI). *Appl. Catal., B* **2017**, *207*, 404−411.
(46) Lawrence, A. L.; Adlington, R. M.; Baldwin, J. E.; Lee, V.; Kershaw, J. A.; Thompson, A. L. A Short Biomimetic Synthesis of the Meroterpenoids. *Org. Lett.* **2010**, *12*, 1676−1679.
(47) Paolesse, R.; Nardis, S.; Venanzi, M.; Mastroianni, M.; Russo, M.; Fronczek, F. R.; Vicente, M. G. H. Vilsmeier Formylation of 5,10,15-Triphenylcorrole: Expected and Unusual Products. *Chem. - Eur. J.* **2003**, *9*, 1192−1197.
(48) Schwab, M. G.; Fassbender, B.; Spiess, H. W.; Thomas, A.; Feng, X.; Müllen, K. Catalyst-free Preparation of Melamine-Based Microporous Polymer Networks through Schiff Base Chemistry. *J. Am. Chem. Soc.* **2009**, *131*, 7216−7217.
(49) Frisch, M. J.; Trucks, G. W.; Schlegel, H. B.; Scuseria, G. E.; Robb, M. A.; Cheeseman, J. R.; Scalmani, G.; Barone, V.; Mennucci, B.; Petersson, G. A.; et al. *Gaussian 09*, revision B.01; Gaussian, Inc.: Wallingford, CT, 2010.
(50) Dutton, C. C.; Dows, D. A.; Eikey, R.; Evans, S.; Beaudet, R. A. The Rovibrational Spectrum and Structure of the Weakly Bound CO_2-CS_2 Complex. *J. Phys. Chem. A* **1998**, *102*, 6904−6909.
(51) Ching, J. C.; Schlemper, E. O. Slightly constrained O—O hydrogen bond. Crystal Structure of A Tetradentate Alpha-Amine Oxime Complex of Nickel(II). *Inorg. Chem.* **1975**, *14*, 2470−2474.
(52) Tognetti, V.; Joubert, L. Density Functional Theory and Bader's Atoms-in-Molecules Theory: Towards A Vivid Dialogue. *Phys. Chem. Chem. Phys.* **2014**, *16*, 14539−14550.
(53) Bader, R. F. W.; Matta, C. Atoms in Molecules as Non-Overlapping, Bounded, Space-Filling Open Quantum Systems. *Found. Chem.* **2013**, *15*, 253−276.
(54) Bader, R. F. W. The Density in Density Functional Theory. *J. Mol. Struct.: THEOCHEM* **2010**, *943*, 2−18.
(55) Hernández-Trujillo, J.; Cortes-Guzman, F.; Fang, D.-C.; Bader, R. F. W. Forces in Molecules. *Faraday Discuss.* **2007**, *135*, 79−95.
(56) Bader, R. F. W. Everyman's Derivation of the Theory of Atoms in Molecules. *J. Phys. Chem. A* **2007**, *111*, 7966−7972.
(57) Bader, R. F. W. A Quantum Theory of Molecular Structure and its Applications. *Chem. Rev.* **1991**, *91*, 893−928.
(58) Bhunia, S.; Bhanja, P.; Das, S. K.; Sen, T.; Bhaumik, A. Triazine Containing N-Rich Microporous Organic Polymers for CO_2 Capture and Unprecedented CO_2/N_2 selectivity. *J. Solid State Chem.* **2017**, *247*, 113−119.
(59) Uribe-Romo, F. J.; Hunt, J. R.; Furukawa, H.; Klöck, C.; O'Keeffe, M.; Yaghi, O. M. A Crystalline Imine-Linked 3-D Porous Covalent Organic Framework. *J. Am. Chem. Soc.* **2009**, *131*, 4570−4571.
(60) Song, W.-C; Xu, X.-K; Chen, Q.; Zhuang, Z.-Z; Bu, X.-H. Nitrogen-Rich Diaminotriazine-Based Porous Organic Polymers for Small Gas Storage and Selective Uptake. *Polym. Chem.* **2013**, *4*, 4690−4696.
(61) Centomo, P.; Zecca, M.; Zoleo, A.; Maniero, A. L.; Canton, P.; Jerabek, K.; Corain, B. Cross-Linked Polyvinyl Polymers versus Polyureas as Designed Supports for Catalytically Active M_0 Nanoclusters Part III. Nanometer Scale Structure of the Cross-Linked Polyurea Support Encat 30 and of the Pd^{II}/Encat 30 and Pd^0/Encat 30NP Catalysts. *Phys. Chem. Chem. Phys.* **2009**, *11*, 4068−4076.
(62) Li, L.; Cai, Z. X.; Wu, Q. H.; Lo, W. Y.; Zhang, N.; Chen, L. X.; Yu, L. P. Rational Design of Porous Conjugated Polymers and Roles of Residual Palladium for Photocatalytic Hydrogen Production. *J. Am. Chem. Soc.* **2016**, *138*, 7681−7686.
(63) Weng, J. Y.; Xu, Y. L.; Song, W.-C.; Zhang, Y. H. Tuning the Adsorption and Fluorescence Properties of Aminal-Linked Porous Organic Polymers Through N-Heterocyclic Group Decoration. *J. Polym. Sci., Part A: Polym. Chem.* **2016**, *54*, 1724−1730.
(64) Raveendran, P.; Ikushima, Y.; Scott L. Wallen, S. L. Polar Attributes of Supercritical Carbon Dioxide. *Acc. Chem. Res.* **2005**, *38*, 478−485.
(65) Queen, W. L.; Hudson, M. R.; Bloch, E. D.; Mason, J. A.; Gonzalez, M. I.; Lee, J. S.; Gygi, D.; Howe, J. D.; Lee, K.; Darwish, T. A.; James, M.; Peterson, V. K.; Teat, S. J.; Smit, B.; Neaton, J. B.; Long, J. R.; Brown, C. M. Comprehensive Study of Carbon Dioxide Adsorption in The Metal-Organic Frameworks M_2(dobdc) (M = Mg, Mn, Fe, Co, Ni, Cu, Zn). *Chem. Sci.* **2014**, *5*, 4569−4581.
(66) Pal, A.; Chand, S.; Elahi, S. M.; Das, M. C. A Microporous MOF with a Polar Pore Surface Exhibiting Excellent Selective Adsorption of CO_2 from CO_2-N_2 and CO_2-CH_4 Gas Mixtures with High CO_2 Loading. *Dalton Trans.* **2017**, *46*, 15280−15286.
(67) Bu, Y.; Cao, Z. Structures and Bonding Character of Ge···CO Weakly Bonding Complexes. *J. Phys. Chem. B* **2002**, *106*, 1613−1621.

DOI: 10.1021/acsami.8b05849
ACS Appl. Mater. Interfaces 2018, 10, 23813−23824